Project FORTE - Nuclear Thermal Hydraulics Research & Development

SCWR Thermal Hydraulics Benchmark Study

August 2019

FNC 53798/49080R Issue 1

FRAZER-NASH CONSULTANCY

SYSTEMS AND ENGINEERING TECHNOLOGY

An introduction to Project FORTE

The Department for Business, Energy and Industrial Strategy (BEIS) has tasked Frazer-Nash Consultancy and its partner organisations to deliver the first phase of a programme of nuclear thermal hydraulics research and development.

Phase 1 of the programme comprises two parts:

- The specification and development of innovative thermal hydraulic modelling methods and tools; and
- The specification of a new United Kingdom thermal hydraulics test facility.

The work is intended to consider all future reactor technologies including Gen III+, small modular reactors and advanced reactor technologies.

Our project partners

The team is led by Frazer-Nash Consultancy and includes:

FRAZER-NASH CONSULTANCY

The University Of Sheffield.

EDF ENERGY

Westinghouse

MANCHESTER 1824
The University of Manchester

Science & Technology Facilities Council

For more information, visit www.innovationfornuclear.co.uk/nuclearthermalhydraulics.html

Executive Summary

To increase the confidence of thermal hydraulics modelling in nuclear applications, a number of experiment-based benchmarking exercises have been launched by various international organisations, such as OECD/NEA, IAEA and EPRI, to assess the quality and performance of the existing numerical tools. These provide good opportunities for the nuclear thermal hydraulics community to evaluate the performance of the models developed and to demonstrate how these models can be used for nuclear applications. Additionally, UK participation in international benchmarking activities promotes UK nuclear thermal hydraulics in an international context, potentially leading to future opportunities for collaboration.

This report describes work to evaluate the performance of an open-source CFD code (Code_Saturne) currently used in the UK nuclear industry for conditions including strongly buoyancy-influenced flows through participation in a benchmarking exercise organised by the IAEA Coordinated Research Project (CRP) in SuperCritical Water-cooled Reactor (SCWR) thermal-hydraulics (Project Code i31025)[1]. The specific choice of benchmarking exercise was dictated by the need to align the timing of the exercise with this project.

This work includes the development of a resolved CFD model based on an existing test facility incorporating a 2x2 SCWR bundle. Numerical simulations have been performed to assess the ability of Code_Saturne to predict supercritical flows and to further develop the understanding of the thermal-hydraulic phenomena relevant to SCWRs. To increase the value of the study, an additional comparison has also been carried out using the commercial CFD code ANSYS FLUENT.

Whilst the benchmark has released data for the two subcritical flow experiments, the data for the supercritical flow experiments has not yet been released (thereby allowing participants to produce ‘blind’ predictions). Despite this, numerical results are presented in this report for both supercritical cases

Differences were seen in the numerical predictions of the two CFD codes with nominally the same modelling setup under both subcritical and supercritical conditions. The reason for this is thought to be due to differences in the implementation of the k-ω SST turbulence model in the two codes. However, the results of both codes lie within the range of available data from the subcritical experiments.

The numerical simulations predict the occurrence of flow laminarisation and heat transfer deterioration within the boundary layer in both of the mixed convection cases.The flow is found to be very sensitive to the thermal environment at supercritical conditions and becomes unstable as it passes through the spacer grid. This helps the initially suppressed turbulence, due to buoyancy, to re-develop and dominate the flow downstream of the spacer grid, leading to a significant reduction in local wall temperature. Such phenomena are of significant importance to the design and optimisation of nuclear reactors and need to be predicted accurately.

The supercritical predictions will be compared to the experimental data and assessed in detail in the CRP report which will be published with all simulation results (including those presented in this report). By participating in this study, this work has raised the profile of the UK internationally and provides technical information of value to Gen-IV reactor developers.

[1] https://www.iaea.org/projects/crp/i31025

Contents

1 Introduction

In order to obtain a cleaner, safer and more efficient future nuclear energy source, the Generation IV International Forum was launched and six designs of nuclear reactor systems have been selected for consideration, amongst which the SuperCritical Water-cooled Reactor (SCWR) is the only water-cooled reactor. Such reactors have the advantage of high thermal efficiency, compact system structure and low capital cost [1, 2]. As opposed to subcritical conditions, heat transfer behaviour of supercritical fluid shows some surprising characteristics due to drastic changes in thermal-physical properties, such as density, specific heat, dynamic viscosity and thermal conductivity in the vicinity of the pseudo-critical temperature [3, 4]. Flows in such conditions are very sensitive to the thermal and structural environment and tend to show sudden changes, which poses a great challenge to the prediction of this process and thus the design of the SCWR.

One of the most significant concerns in using a supercritical fluid as a reactor primary circuit coolant is 'heat transfer deterioration.' This effect is caused by the large variation in physical properties of a fluid (e.g. density and thermal conductivity) near the pseudo-critical line [5]. A reduction in heat transfer can cause undesirably high solid wall temperatures that put constraints on the material that the reactor and/or fuel is made of. Experimental studies on heat transfer of supercritical pressure fluids are still limited due to the technical difficulty and high cost of equipment. However, the rapid development of numerical techniques and the increase of computing capacity now allows the simulation of flows under supercritical conditions.

In the past decades, state-of-the-art Computational Fluid Dynamics (CFD) has been used by many researchers to study flow and heat transfer of supercritical fluids in simple geometries, including circular pipes [6 - 12], plane channels [13, 14] and annular channels [15, 16], which have greatly enhanced the understanding of this phenomenon. However, these studies could not reach a consensus on the choice of a suitable turbulence model for supercritical flow simulations, as it has been found that the quality of the results produced by the various turbulence models used in these works changes significantly from case to case, as they are flow and geometry dependent [17]. Among the various turbulence models tested, the low Reynolds number k-ω SST model is believed by some researchers [15, 18 - 20] to show better results than other RANS models in simulating supercritical flows when the wall region is well resolved (y^+~1.0).

In addition, high-fidelity methods like Direct Numerical Simulation (DNS) have also been used to produce detailed information to enhance understanding of heat transfer deterioration and to assist the improvement of turbulence models [6, 21 - 24]. However, such methods are currently still restricted to relatively low Reynolds numbers and simple geometries due to the huge computational cost.

With the accumulation of knowledge derived from these studies, researchers began to study heat transfer in "real" SCWR fuel channels to assist in engineering development. One of the simplest ways is to make use of the data obtained previously on simple geometries, e.g., in the case of a circular tube. Correlations have been developed assuming that the heat transfer behaviour in an SCWR sub-channel is similar to a corresponding tube of equal hydraulic diameter. However, this is not reliable in many cases, e.g., the heat transfer deterioration in tubes may not occur in an SCWR bundle with spacer grids at similar flow and thermal conditions [25]. Therefore, experimental or numerical studies can provide more useful information if they are based on a representative configuration that closely resembles the whole reactor bundle. The most intensively studied configuration in open literature is the single SCWR sub-channel

due to its low computing cost [26 - 29]. In order to capture the complex exchanges among sub-channels, studies have also been widely carried out on configurations including multiple sub-channels, such as 2×2 square bundle and 7-rod hexagon bundle [17, 30]. The results obtained indicated that both the geometry and orientation of the rod bundle can have a significant effect on the flow and thermal behaviour in an SCWR.

This study is part of the blind benchmarking excise organised by an IAEA Coordinated Research Project (CRP) on SCWR (Project code i31025) aimed at improving the understanding of the thermal-hydraulic phenomena relevant to SCWRs and assessing the predictive capability of the numerical tools and methods. The benchmarking data was produced in an experimental facility with a 2×2 rod bundle operated at conditions resembling those of an “industrial” SCWR. The most interesting parameter in this benchmarking excise is the cladding temperature that was measured using embedded thermocouples mounted at various axial and circumferential locations in the experimental rig. Details of the experiment are given in Section 2.

Experimental data are currently available only for two subcritical cases, but not yet available for the supercritical cases studied. In this report, simulations were carried out using two different CFD packages, one is an open-source CFD code Code_Saturne (v5.0) developed by EDF R&D [31], and the other is the commercial code ANSYS FLUENT (v16.1). Mesh, turbulence model and numerical schemes used in these two packages were kept the same where possible so that ‘user effects’ are minimised and the sensitivity of the results to numerical tools could be assessed. The numerical approach is described in Section 3 and the results of the analysis are presented and discussed in Section 4. The conclusions are summarised in Section 5.

2 Description of Experiment

2.1 Test Facility

The benchmarking experiment was conducted in a University of Wisconsin (UW) high-pressure heat transfer test facility located in Stoughton, Wisconsin, US [32]. It consists of a primary flow loop where the coolant is pumped into a heated test section and a secondary flow loop used for heat removal. Figure 1 is a schematic of the primary flow loop. The maximum operating pressure and temperature of the system are 25 MPa and 400 °C, respectively.

The test section is a vertical square duct enclosing a 2×2 rod bundle, providing a maximum of 400 kW of heat to the fluid. The rod bundle is aligned by spacer grids which have the same form factor as the adjacent square channel, allowing them to minimise the reduction of the flow area which is about 17% of the total flow area. Therefore, they do not cause significant disturbances to the flow.

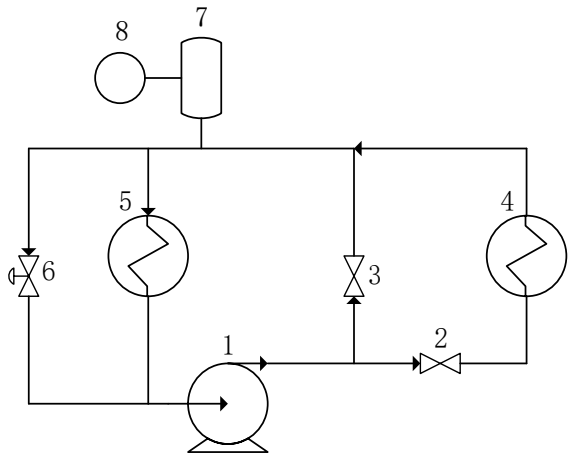

1. High pressure pump 2. Orifice flow meter 3. Bypass orifice 4. Heated test section
5. Heat exchange 6. Bypass valve 7. Pressurizer/Accumulator 8. Argon gas cylinder

Figure 1: Schematic of the primary flow loop in the test facility

Six spacer grids are welded in between five duct segments to create the full length of the test section which is 2151.5 mm. It is slightly longer than the heated length which is 2000 mm. The locations of the spacer grids with respect to the start of the heated section can be found in Table 1.

Table 1: Locations of the spacer grids

Grid No.	Axial location (mm from the start of the heated section)	
	Start	End
1	-97.10	-90.75
2	327.54	339.27
3	757.74	769.63
4	1187.89	1199.01
5	1617.88	1628.68
6	2048.03	2054.38

Figure 2 shows one of the five sections. Two spacer grids are located outside the range of the heated section. The first one is before the start of the heated section and the second one is after the end of the heated section. Figure 3 shows the dimensions of the cross-section of the test section and corresponding spacer grids. The total flow area is 3.9 cm^2 and the pitch-to-diameter ratio is 1.33.

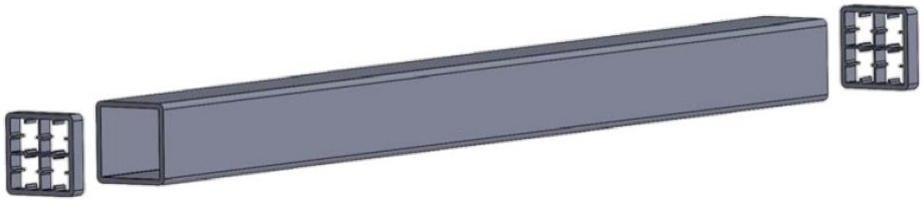

Figure 2: Sketch of one of the five duct segments in the test section

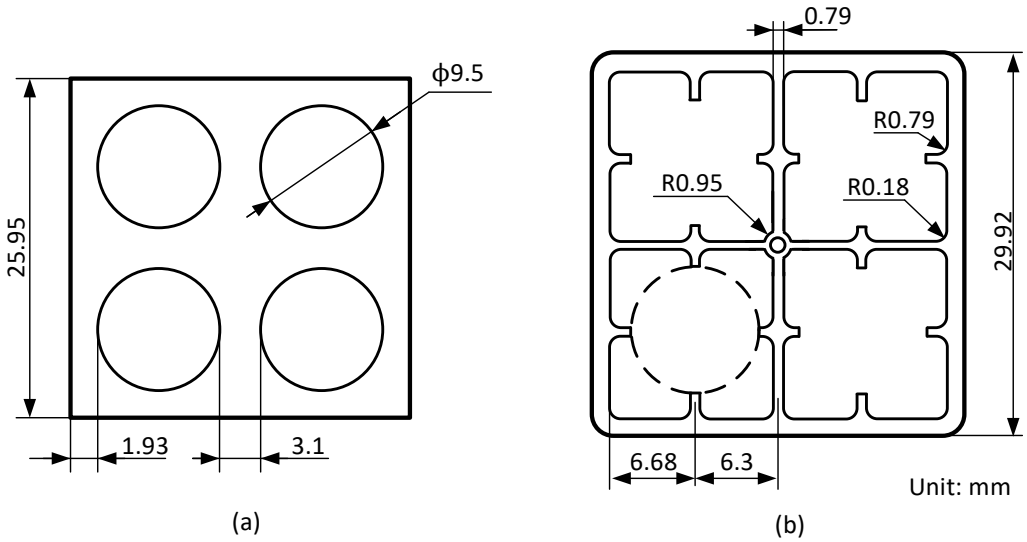

Figure 3: Dimensions of (a) the flow channel of the test section and (b) the spacer grids

An axial cosine power profile is provided by the heater in the experiment to simulate the power distribution during fission reactions within nuclear fuel rods. The power profile is given by the following equation,

$$\dot{q}(z) = q_{av}\left\{\theta_0 + \theta_1 \cos\left[2\theta_2\left(\frac{z}{L} - 0.5\right)\right]\right\} \quad (1)$$

where q_{av} is the mean heating power per rod, z is the axial height from the start of the heated section, L is the total length of the heated section (L = 2 m), θ_0, θ_1 and θ_2 are constants:

θ_0 = 0.8187458177

θ_1 = 0.6812541823

θ_2 = 2.436354311

Ten embedded thermocouples are mounted at various axial and circumferential locations on each heated rod to measure the solid surface temperature, whilst eight bulk thermocouples are used to monitor the bulk fluid temperature at six different axial locations. The last axial location is

monitored by three bulk thermocouples each 90° apart. Details can be found in Figure 4 and Table 2.

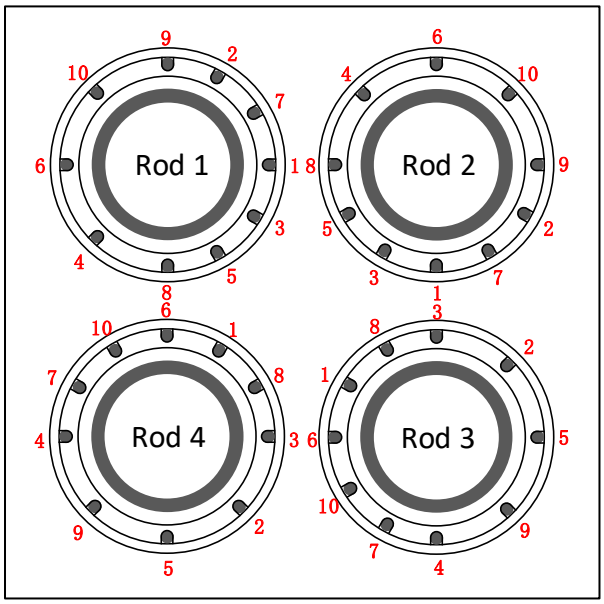

Figure 4: Circumferential locations of the embedded thermocouples

Table 2: Locations of the embedded and bulk thermocouples

	Rod Internal Thermocouples			Bulk Thermocouples	
TC No.	Angular location (°)		Axial location (mm from start of the heated section)	Bulk TC No.	Axial location (mm from start of the heated section)
	Rods 1/2	Rods 3/4	Rods 1/2/3/4		
1	0	330	961.9	1	579
2	60	225	1038.1	2	1038
3	330	270	1333.5	3	1333
4	225	90	1333.5	4	1462
5	300	180	1462.0	5	1538
6	180	0	1462.0	6/7/8	1778
7	60	60	1538.2		
8	270	300	1778.0		
9	90	135	1778.0		
10	135	30	1974.6		

2.2 Test Cases

Four cases have been studied, which can be divided into two groups in terms of operating pressure. Group I includes two ‘subcritical’ cases, namely Case-A and Case-B, in which the operating pressure is around 8 MPa, far below the critical pressure of water (22.1 MPa). The incompressibility of liquids at ‘normal’ conditions means that the buoyancy force caused by density variation is thought to play an insignificant role in comparison to the pressure and viscous forces. Therefore, it is to be expected that numerical predictions of wall temperatures in such cases will compare closely with the experimental data, as the current CFD tools are relatively mature in handling single-phase forced convection problems.

In contrast, the operating pressure is 25 MPa in the Group II cases (Case-C and Case-D), so they are ‘supercritical’ cases. The q/G ratios (heat flux/mass flux) used in the Group II cases are

much higher than those used in the Group I cases in order to ensure that the pseudo-critical temperature (384.9 °C) can be reached at certain heights within the heated channel. As such, the complex physics related to the large physical property changes of a fluid crossing through the pseudo-critical point could cause potential difficulties in numerical simulations. This may also lead to unexpected deviations when comparing the predictions of different numerical tools due to the high sensitivity of the flow to details of modelling tool and mesh setups. An overview of the cases is given in Table 3. It should be noted that higher heating power is imposed in Case-C, though, the anticipated temperature increase is lower than that of Case-D due to a lower q/G ratio. Thus, the stronger buoyancy effect would be expected to occur in Case-D.

Table 3: Overview of the cases

Group	Case	P_{in} (MPa)	T_{in} (°C)	G (kg/m^2·s)	q_{av} (kW/rod)
I	A	8.26	121.8	2201	10.07
	B	8.28	149.6	1447	24.96
II	C	25.0	346.0	844	47.8
	D	25.0	340.0	450	32.9

3 Numerical Approach

Considering the fact that the low Reynolds number k-ω SST model has been found to perform the best in predicting supercritical flows among various RANS models in a number of studies [15, 18, 20], it has been used to account for turbulence throughout this study. The symmetric nature of the rod bundle means that it is not necessary to simulate the full geometry. The smallest possible representative section (i.e. 1/8 of the channel) was selected and has been highlighted using red lines in Figure 5(a). Figure 5(b) and Figure 5(c) show a cross-sectional view normal to the stream-wise direction of the extruded mesh at regions with and without a spacer grid, respectively. It should be noted that the geometry of the spacer grids are slightly simplified (some of the fillets are ignored and replaced with straight corners) to reduce the difficulty in mesh generation.

To capture the complex physics in the boundary layer of buoyancy influenced flows, a very fine near-wall grid is used for major solid boundaries (i.e. the outer surfaces of the heated rods and the inner surface of the square duct) to resolve the viscous sub-layer, leading to a total of 10.3 million mesh cells. The heights of the first cell adjacent to the wall surfaces of the heated rods and the square duct are very small (0.0056 mm and 0.0057 mm, respectively) so that the y^+ value for these boundaries can be maintained around 1.0. Additionally, the near wall mesh is composed of 16 hexahedral layers with a growth factor of 1.2. It should be pointed out that the mesh resolution for some of the spacer grid surfaces is relatively low. This is a compromise to ensure the consistency and conformality of the mesh. Such a localised loss in mesh resolution is not expected to affect the overall picture of the results, as the spread of the resulting numerical error is suppressed by diffusion and thus restricted within a short distance from its originated place.

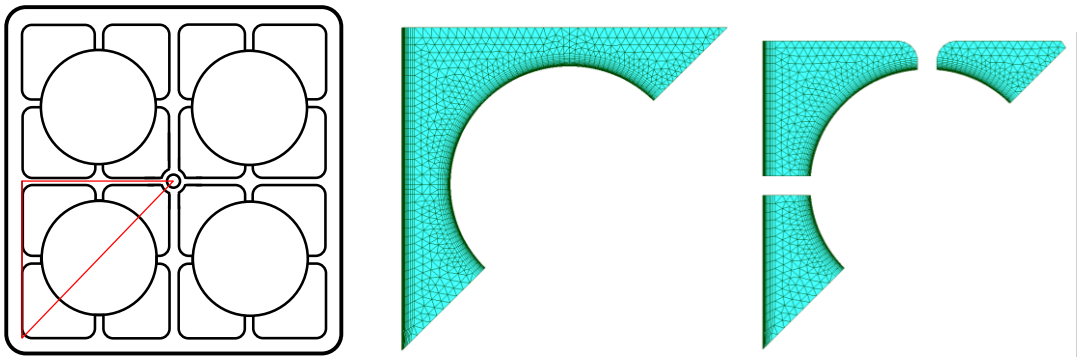

Figure 5: Sketch of the geometry and mesh. (a) 1/8-representative section (highlighted by red lines), (b) cross-section view of the mesh for regions without spacer grid, (c) cross-section view of the mesh for regions with spacer grid

In Code_Saturne, either temperature or enthalpy is available as the field variable for the energy equation. The enthalpy form is selected throughout the simulations since the temperature is insensitive to energy change in the vicinity of the pseudo-critical point due to the extremely high values of the specific heat. A high resolution enthalpy-based physical property table is generated using NIST database REFPROP 9.0 and implemented in Code_Saturne (v5.0) for physical property updates during the simulations. The property table used in Code_Saturne is based on a uniformly distributed enthalpy at intervals of 500 J/kg, leading to a very high density of data points near the pseudo-critical point with the smallest corresponding temperature interval of 0.005 °C. Linear interpolation is used to calculate the material properties between

intervals. In ANSYS FLUENT, the NIST database can be enabled directly as it has been embedded in the version used (v16.1).

A pressure-based transient fractional-step solver is used in both codes for time advancement. Second order schemes are employed with higher priority for spatial discretisation of the momentum and the energy equation. The flow at the inlet is assumed to be fully developed so that a fully developed velocity profile can be imposed. Although this would clearly not be the case in the real experiment, the regions of interest are sufficiently far downstream that the assumptions at inlet will have a negligible effect on the results. A buffer section is added after the last spacer grid to minimise the impact of the outlet boundary condition on the main flow region. All walls are assumed to be non-slip smooth walls. The y^+ value of the first cell for the main walls, e.g. except for the spacer region, is kept around 1.0, especially for Group II cases. Simulations were run on a Tier 2 cluster located at the Science and Technology Facilities Council (STFC) Daresbury Laboratory in the UK. The simulations were typically run using 512 cores.

4 Results and Discussion

Figure 6(a) and Figure 6(b) are comparisons of the axial temperature distribution between simulation results and experimental data for the two subcritical cases of Group I. The bulk temperature and circumferential averaged wall temperature are sampled along the stream-wise direction every 5 mm from the start to the end of the heated section. They are calculated using the following equations,

$$T_{bulk,z_0} = \int_{z=z_0} \rho \mathbf{u} T \cdot d\mathbf{A} \Big/ \int_{z=z_0} \rho \mathbf{u} \cdot d\mathbf{A} \tag{2}$$

$$T_{wall,z_0} = \int_{z=z_0} T dA_s \Big/ \int_{z=z_0} dA_s \tag{3}$$

where **u** is the local velocity vector, **A** is the face vector of the cross-section, A_s is the area of the rod surface.

It can be seen that the bulk temperatures predicted by the two codes both agree well with the experimental data in Group I cases. However, the predicted averaged wall temperatures deviate from each other by a maximum of 5 °C in Case-A and 10 °C in Case-B. The FLUENT results seem to compare slightly better with experiments than those of Code_Saturne; the latter lie around the upper bound of the experimental data range, suggesting that the wall temperature is potentially overestimated slightly.

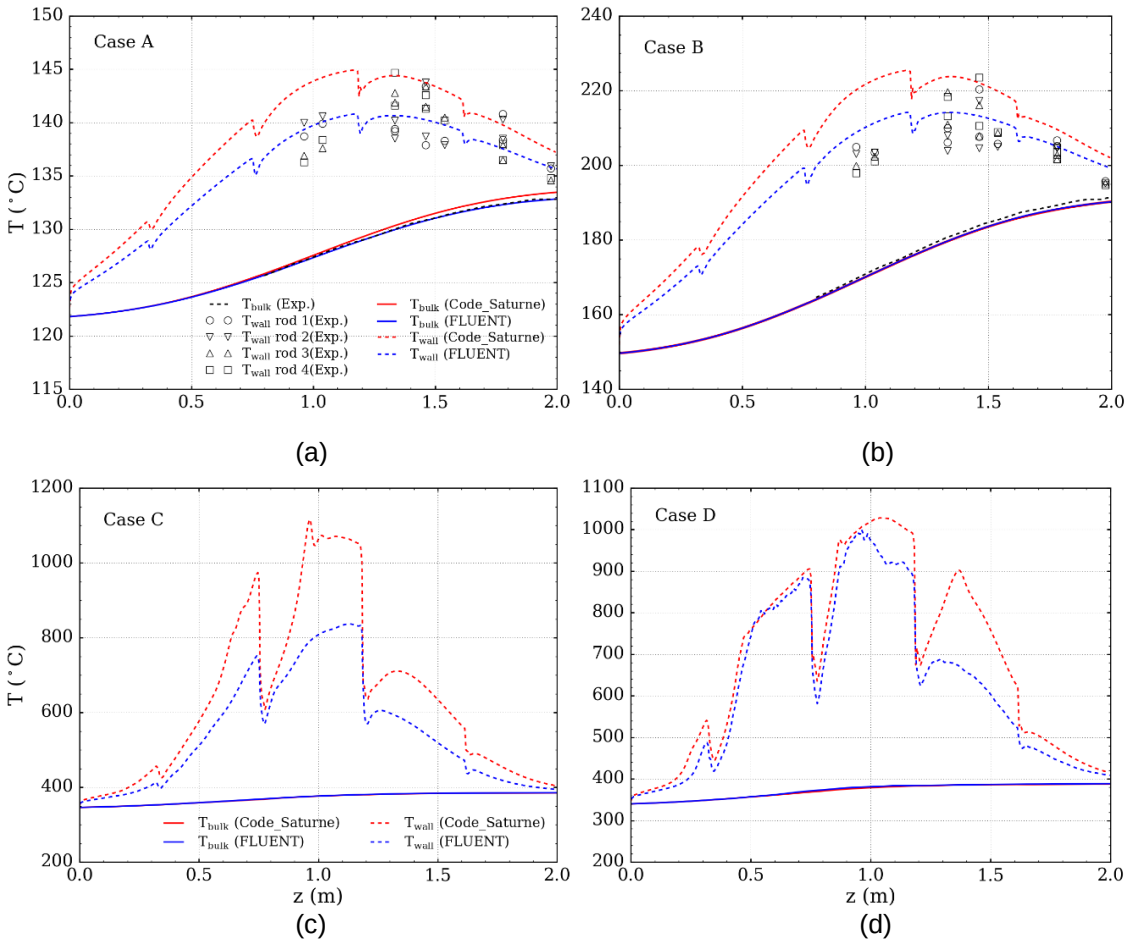

Figure 6: Axial distribution of bulk temperature and circumferential averaged wall temperature of the fuel rod

In general, CFD modelling for the subcritical cases can be performed with higher confidence than the supercritical cases due to the less complex flow physics. However, in practice, the simulation results may still vary slightly from code to code even using nominally the same turbulence model and numerical setups due to potential differences in model implementation and/or related numerical treatments. This is well known in the CFD community and most likely to be the reason why such a difference is observed between the two codes in predicting the rod wall temperatures in both of the subcritical cases.

It is also worth noting that the spacer grids have small but noticeable impacts on the overall distribution of the wall temperature when the fluid passes through the spacer region. The wall temperature reduces suddenly due to the disruption of the thermal boundary layer by the spacer grid and the relatively high turbulent intensities induced in the spacer region. Troughs can be observed at axial locations of 0.3 m, 0.8 m, 1.2 m, and 1.6 m, corresponding to the spacer grids in the heated section (spacer grid II to V).

Compared with the two subcritical cases in Group I, the results of the supercritical cases in Group II show large differences in axial distribution of wall temperature which increases sharply after reaching the pseudo-critical point, leading to a huge difference of up to 600 °C from the bulk temperature, see Figure 6(c) and Figure 6(d). The huge increase in wall temperature can be attributed to flow laminarisation happening in the boundary layer, which impairs the heat transfer therein.

Both Code_Saturne and FLUENT capture this phenomenon, but the latter predicts a much lower level of heat transfer deterioration in Case-C, resulting in a significant deviation in wall temperature prediction from the former. In Case-D, on the other hand, the two codes agree well with each other on the occurrence and development of heat transfer deterioration, but FLUENT predicts an earlier occurrence of recovery. It should also be noted that the laminarised boundary layer is delicate and can be reversed locally by disturbances induced from the spacer grids, leading to wall temperature spikes (i.e. sharp decrease followed by a sharp increase). This phenomenon can be observed in both Case-C and Case-D.

In order to see more clearly the occurrence and development of the flow laminarisation in Group II cases, the axial velocity and the turbulent shear stress have been plotted for the Code_Saturne results along the radial direction at cross-sections of different axial positions. As can be seen in Figure 7(a), for Case-C, the velocity profile starts to flatten at about z=0.9 m due to the near-wall acceleration caused by the buoyancy force, followed by a significant M-shaped profile (e.g. z=1.1 m), and then flattens again (e.g. z=1.5 m and z=1.8 m). Accordingly, the turbulent shear stress experiences firstly a decrease and then increases (see Figure 7(b)), indicating the occurrence of flow laminarisation and recovery.

It should be noted that the recovery that happens here is not like that in a uniform-heating case caused normally by the exaggeration of buoyancy. On the contrary, it is due to the weakened buoyancy effect in the second half of the channel where heating power is diminishing. Correspondingly, Figure 7(c) and Figure 7(d) show the equivalent results for Case-D. The overall picture is similar to that of Case-C, but the suggested buoyancy effect is more significant.

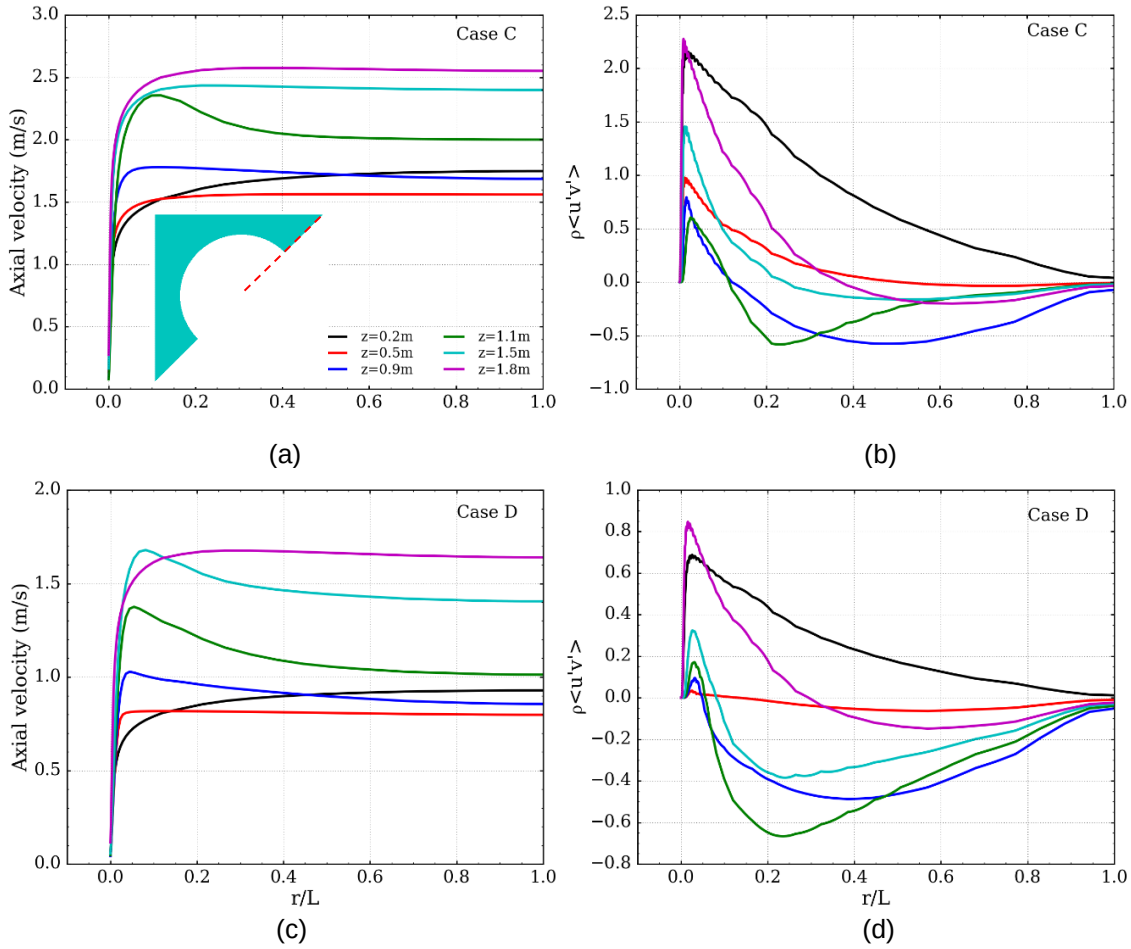

Figure 7: Local axial velocity and turbulent shear stress profiles for Group II cases (Plots are based on Code_Saturne results)

Figure 8(a) shows the axial pressure drop for the four cases. It is to be expected that a linear pressure drop with constant form losses at spacer grids is observed in Case-A and Case-B, since they are purely forced convection flows. In such cases, the flow is expected to be fully developed in between the spacers, thus resulting in a uniform frictional loss. This is no longer the case in Case-C and Case-D in which buoyancy plays an important role and turbulence varies significantly along the flow path. In Case-D, the buoyancy effect is so strong that a negative pressure drop occurs in the higher section of the channel. Where the flow is strongly heated, flow acceleration would also be expected along the duct, due to thermal expansion.

Figure 8 (b) shows the bulk velocity along the axial direction. It can be seen clearly that no significant flow acceleration occurs in the Group I cases since the thermal expansion is negligible. In contrast, the flow accelerates to about twice the magnitude of the initial velocity in both cases of Group II. The flow acceleration is a direct response to the thermal expansion of the fluid, which happens more significantly when the increasing bulk temperature passes through the pseudo-critical point where the fluid becomes gas-like.

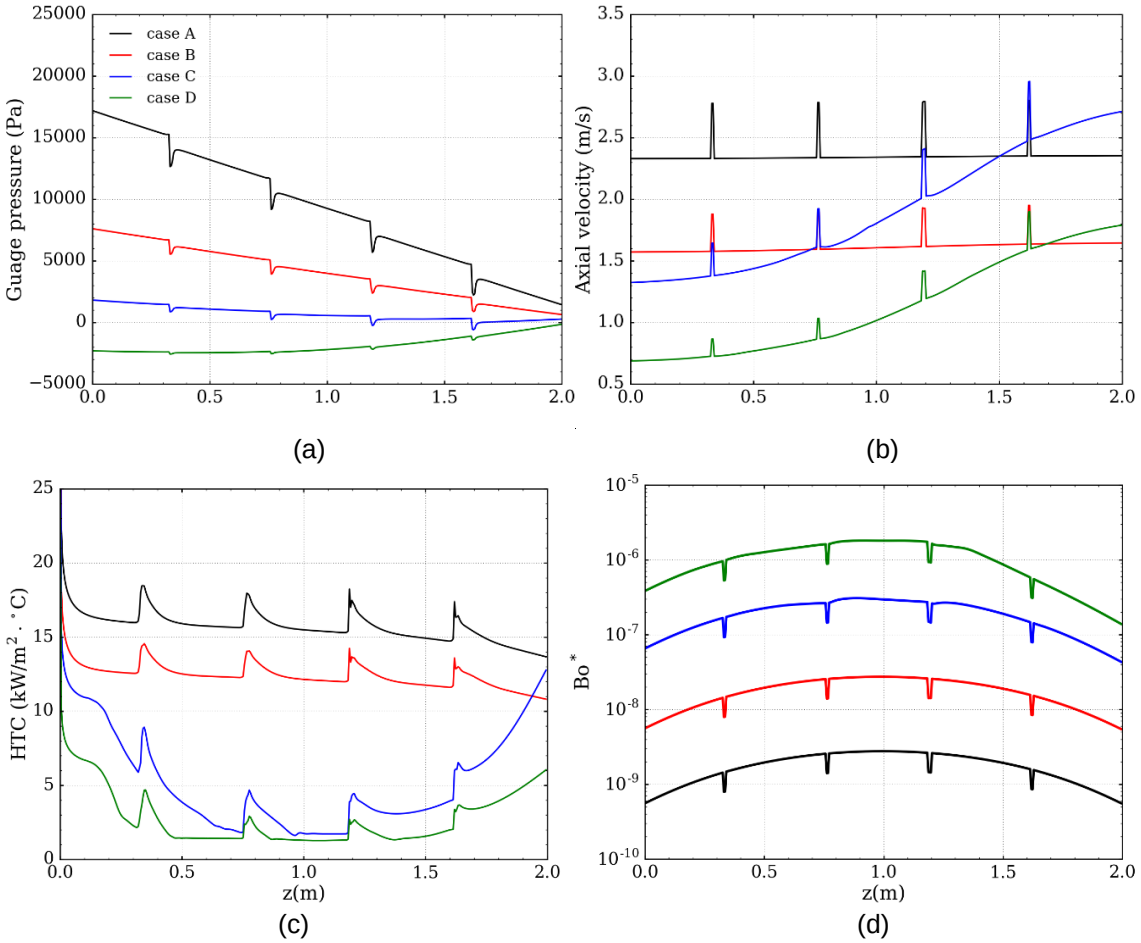

Figure 8: Comparisons of Case A-D (a) axial pressure drop, (b) bulk velocity, (c) heat transfer coefficient and (d) buoyancy parameter (Plots are based on Code_Saturne results)

Flow laminarisation resulting from a distorted velocity profile due to buoyancy is believed to be the reason for the heat transfer deterioration. This is further evaluated using the Heat Transfer Coefficient (HTC) and buoyancy parameter *Bo** (see Equation (4)). The two parameters are plotted along the axial direction for both Group I and Group II cases in Figure 8(c) and Figure 8(d), respectively. In general, the HTC spikes appear around the locations where the spacer grids are installed. This can be attributed to the disruption of the thermal boundary layer and locally enhanced heat transfer related to structure-induced turbulence. For the Group I cases, an overall decrease of less than 10% in HTC can be observed throughout the whole test section, indicating that the heat transfer is not impaired significantly. In contrast, a sharp decrease of about 80% happens in both Group II cases, suggesting the occurrence of heat transfer deterioration.

Correspondingly, Figure 8(d) shows the evolution of the buoyancy parameter along the axial direction for all of the cases studied. It can be seen that only Case-D meets the criterion of $Bo^* > 5.7\times10^{-7}$ in which case the buoyancy effect is significant, although it should be noted that this criterion was established based on normal fluids at atmosphere pressure. In practice, a lower value is suggested to be used in evaluating the buoyancy effect in supercritical pressure fluids [33]. In addition, the recovery of HTC in Group II cases that occurs in the second half of the test section is not due to the increase of the buoyancy effect (which is expected to be

decreasing in these regions according to the distribution of the buoyancy parameter), instead, it is merely due to the reduced heating on the rods.

$$Bo^* = \frac{Gr^*}{\mathrm{Re}^{3.425}\,\mathrm{Pr}^{0.8}} \tag{4}$$

where the Gr* is the Grashof number based on wall heat flux, which is calculated from Equation (5), Re and Pr are the Reynolds number and Prandtl number, respectively.

$$Gr^* = \frac{g\beta q' D_h^{\,4}}{\lambda \nu^2} \tag{5}$$

where g is the acceleration due to gravity, β is the thermal expansion factor, q' is the wall heat flux, D_h is the hydraulic diameter, λ is the thermal conductivity, v is the kinematic viscosity.

5 Conclusions

The primary aim of this benchmark is to enhance the understanding of the underlying physics in buoyancy-aided flows of water at supercritical conditions, which is essential in the design and development of SCWRs.

A numerical model is built-up based on a benchmarking experiment carried out in a 2×2 rod bundle facility operated with water at subcritical and supercritical pressures. The model was first implemented in an open-source CFD code, Code_Saturne, and validated for subcritical conditions, as the relevant experimental data had already been released to the benchmarking participants. In order to assess and compare the accuracy of different CFD codes, the well-known commercial code ANSYS FLUENT was also used to generate simulation results with the same mesh and model setup.

Overall, both codes produce acceptable results for the subcritical cases, although a difference in wall temperature prediction is observed between them, which may be due to the potential differences in model implementation and/or related numerical treatments. The experimental data are still not available for the supercritical cases. Despite this, numerical results are presented in this report for both supercritical cases. The numerical simulations predict the occurrence of flow laminarisation and heat transfer deterioration within the boundary layer in both of the mixed convection cases. These predictions will be compared to the experimental data and assessed in detail in the CRP report which will be published with all simulation results (including those presented in this report).

The secondary aim of this work is to evaluate the performance of the open-source CFD tool Code_Saturne in simulating supercritical flows. Through the simulations, the code is found to be stable and robust with the k-ω SST turbulence model, even though some localised low mesh resolutions are used on non-important walls as a compromise to ensure mesh conformality. Code_Saturne generally agrees well with FLUENT in predicting some of the major physics in mixed convections, such as flow laminarisation and heat transfer deterioration, but tends to be more responsive to buoyancy effects and thus gives higher wall temperature predictions. The reason for this is thought to be due to differences in the implementation of the k-ω SST turbulence model in the two codes.

By participating in this study, this work has raised the profile of the UK internationally and provides technical information of value to Gen-IV reactor developers.

6 References

1. G. Heusener, U. Muller, T. Schulenberg, & D. Squarer, A European development program for a High Performance Light Water Reactor (HPLWR). *Proceedings of the 1st International Symposium on Supercritical Water Cooled Reactor Design and Technology*, (Tokyo, 2000).

2. Y. Oka & S. Koshizuka, Supercritical-pressure, once-through cycle light water cooled reactor concept. Journal of Nuclear Science and Technology, 38 (2001) 1081-1089.

3. J. D. Jackson & W. B. Hall, Forced convection heat transfer to fluids at supercritical pressure. Turbulent Forced Convection in Channels and Rod Bundles (1979), pp.563–611.

4. J. D. Jackson & W. B. Hall, Influences of buoyancy on heat transfer to fluids flowing in vertical tubes under turbulent conditions. Turbulent Forced Convection in Channels and Rod Bundles (1979), pp.613–640.

5. R. S. Abdulmohsin & M. H. Al-Dahhan, Axial dispersion and mixing phenomena of the gas phase in a packed pebble-bed reactor. Annals of Nuclear Energy, 88 (2016) 100-111.

6. J. H. Bae, J. Y. Yoo, & H. Choi, Direct numerical simulation of turbulent supercritical flows with heat transfer. Physics of Fluids, 17 (2005) 105104.

7. S. He, P. X. Jiang, R. Shi, W. S. Kim, & J. D. Jackson, Computational study of convective heat transfer to CO2 at supercritical pressure in a vertical mini tube. Proceedings of the 2nd International Conference on Microchannels and Minichannels, (New York, 2004).

8. S. He, P.-X. Jiang, Y.-J. Xu, R.-F. Shi, W. S. Kim, & J. D. Jackson, A computational study of convection heat transfer to CO2 at supercritical pressures in a vertical mini tube. International Journal of Thermal Sciences, 44 (2005) 521-530.

9. S. He, W. S. Kim, & J. H. Bae, Assessment of performance of turbulence models in predicting supercritical pressure heat transfer in a vertical tube. International Journal of Heat and Mass Transfer, 51 (2008) 4659-4675.

10. S. He, W. S. Kim, P. X. Jiang, & J. D. Jackson, Simulation of mixed convection heat transfer to carbon dioxide at supercritical pressure. Proceedings of the Institution of Mechanical Engineers Part C: Journal of Mechanical Engineering Science, 218 (2004) 1281-1296.

11. M. Jaromin & H. Anglart, A numerical study of heat transfer to supercritical water flowing upward in vertical tubes under normal and deteriorated conditions. Nuclear Engineering and Design, 264 (2013) 61-70.

12. L. Liu, Z. Xiao, X. Yan, X. Zeng, & Y. Huang, Heat transfer deterioration to supercritical water in circular tube and annular channel. Nuclear Engineering and Design, 255 (2013) 97-104.

13. M.-T. Kao, M. Lee, Y.-M. Ferng, & C.-C. Chieng, Heat transfer deterioration in a supercritical water channel. Nuclear Engineering and Design, 240 (2010) 3321-3328.

14. M. Sharabi, W. Ambrosini, S. He, & J. D. Jackson, Prediction of turbulent convective heat transfer to a fluid at supercritical pressure in square and triangular channels. Annals of Nuclear Energy, 35 (2008) 993–1005.

15. L. Liu, Z. Xiao, X. Yan, X. Zeng, & Y. Huang, Numerical simulation of heat transfer deterioration phenomenon to supercritical water in annular channel. Annals of Nuclear Energy, 53 (2013) 170-181.

16. D. Ma, T. Zhou, & B. Li, Diametrical effects of supercritical water heat transfer in annular channels. Proceedings of 17th International Topical Meeting on Nuclear Reactor Thermalhydraulics, (Xi'an, 2017).

17. K. Podila & Y. Rao, CFD modelling of supercritical water flow and heat transfer in a 2×2 fuel rod bundle. Nuclear Engineering and Design, 301 (2016) 279-289.

18. D. Palko & H. Anglart, Theoretical and numerical study of heat transfer deterioration in high performance light water reactor. Science and Technology of Nuclear Installations, (2008) 1-5.

19. T. Schulenberg & D. C. Visser, Thermal-hydraulics and safety concepts of supercritical water cooled reactors. Nuclear Engineering and Design, 264 (2013) 231-237.

20. Y. Zhu, Numerical Investigation of the Flow and Heat Transfer within the Core Cooling Channel of a Supercritical Water Reactor. PhD Thesis, (2010).

21. H. Nemati, A. Patel, B. J. Boersma, & R. Pecnik, Mean statistics of a heated turbulent pipe flow at supercritical pressure. International Journal of Heat and Mass Transfer, 83 (2015) 741-752.

22. H. Nemati, A. Patel, B. J. Boersma, & R. Pecnik, The effect of thermal boundary conditions on forced convection heat transfer to fluids at supercritical pressure. Journal of Fluid Mechanics, 800 (2016) 531-556.

23. W. Wang & S. He, Direct numerical simulation of fluid flow at supercritical pressure in a vertical channel. Proceeding of 16th International Topical Meeting on Nuclear Reactor Thermal Hydraulics, (Chicago, 2015).

24. J. H. Bae, J. Y. Yoo, H. Choi, & D. M. McEligot, Effects of large density variation on strongly heated internal air flows. Physics of Fluids, 18 (2006) 075102.

25. L. Leung & Y. Rao, A strategy in developing heat-transfer correlation for fuel assembly of the Canadian super-critical water-cooled reactor. Proceeding of 7th International Symposium on Supercritical Water-Cooled Reactors, (Helsinki, 2015).

26. E. Ampomah-Amoako, E. H. K. Akaho, B. J. B. Nyarko, & W. Ambrosini, Analysis of flow stability in nuclear reactor subchannels with water at supercritical pressures. Annals of Nuclear Energy, 60 (2013) 396-405.

27. H. Y. Gu, X. Cheng, & Y. H. Yang, CFD analysis of thermal-hydraulic behaviour of supercritical water in sub-channels. Nuclear Engineering and Design, 240 (2010) 364-374.

28. K. Podila & Y. F. Rao, CFD analysis of flow and heat transfer in Canadian supercritical water reactor bundle. Annals of Nuclear Energy, 75 (2015) 1-10.

29. M. M. Rahman, J. Dongxu, M. S. Beni, H. C. Hei, W. He, & J. Zhao, Supercritical water heat transfer for nuclear reactor applications: a review. Annals of Nuclear Energy, 97 (2016) 53-65.

30. M. Rohde, J. W. R. Peeters, A. Pucciarelli, A. Kiss, Y. F., Rao, E. N. Onder, P. Muehlbauer, A. Batta, M. Hartig, V. Chatoorgoon, R. Thiele, D. Chang, S. Tavoularis, D. Novog, D. McClure, M. Gradecka, & K. Takase, Numerical Benchmark Study on

Supercritical Water Heat Transfer Experiments in a 7-Rod Bundle. Journal of Nuclear Engineering and Radiation Science, 2 (2016) 021012.

31. Y. Fournier, J. Bonelle, C. Moulinec, Z. Shang, A.G. Sunderland, & J.C. Uribe, Optimizing Code_Saturne computations on Petascale systems. Computers & Fluids, 45 (2011) 103-108.

32. L. Kate, M. Anderson, CFD Benchmark Analysis for 2x2 Fuel Rod Bundle. (2016).

33. S. He, W. S. Kim, & J. D. Jackson, A computational study of convective heat transfer to carbon dioxide at a pressure just above the critical value. Applied Thermal Engineering, 28 (2008) 1662-1675.

DOCUMENT INFORMATION

Project : Project FORTE - Nuclear Thermal Hydraulics Research & Development

Report Title : SCWR Thermal Hydraulics Benchmark Study

Client : Department for Business, Energy and Industrial Strategy (BEIS)

Report No. : FNC 53798/49080R

Issue No. : 1

Date : August 2019

Compiled By : Dr B. Liu
(University of Sheffield)

Verified By : Professor S. He
(University of Sheffield)

Approved By : C. Howlett

Originating Office: FRAZER-NASH CONSULTANCY LIMITED
The Cube, 1 Lower Lamb Street, Bristol, BS1 5UD
T: +44 (0)117 9226242 F: +44 (0)117 9468924 W: www.fnc.co.uk

Frazer-Nash Consultancy Ltd
The Cube
1 Lower Lamb Street
Bristol
BS1 5UD

T +44 (0)117 9226242
F +44 (0)117 9468924

www.fnc.co.uk

Offices at:
Bristol, Burton-on-Trent, Dorchester,
Dorking, Glasgow, Plymouth, Warrington
and Adelaide